

Perspective: Non-conventional Force Fields for Applications in Spectroscopy and Chemical Reaction Dynamics

Debasish Koner,^{†,§} Seyedeh Maryam Salehi,^{†,§} Padmabati Mondal,^{‡,§} and Markus Meuwly^{*,¶}

[†]*Department of Chemistry, University of Basel, Klingelbergstrasse 80, 4056 Basel, Switzerland*

[‡]*Indian Institute of Science Education and Research (IISER) Tirupati, Karakambadi Road, Mangalam, Tirupati-517507, Andhra Pradesh, India.*

[¶]*Department of Chemistry, University of Basel, Klingelbergstrasse 80, 4056 Basel, Switzerland*

Department of Chemistry, Brown University, Providence, RI, USA

§These authors contributed equally.

E-mail: m.meuwly@unibas.ch

Abstract

Extensions and improvements of empirical force fields are discussed in view of applications to computational vibrational spectroscopy and reactive molecular dynamics simulations. Particular focus is on quantitative studies which make contact with experiments and provide complementary information for a molecular-level understanding of processes in the gas phase and in solution. Methods range from including multipolar charge distributions to reproducing kernel Hilbert space approaches and machine learned energy functions based on neural networks.

Introduction

Atomistic Simulations have become a powerful way to provide molecular-level insights into gas- and condensed-phase properties of physico-chemical systems and to interpret and complement experiments. Much of the progress is directly related to the dramatically increased capabilities of modern computer infrastructure. Nevertheless, the field is still far from solving general problems by running either sufficiently long (quasi-)classical trajectories or large-scale quantum dynamics simulations in order to characterize a particular system. Even for an atom+diatom system the comprehensive calculation of all state-to-state cross sections is a formidable task and brute-force sampling is a serious computational undertaking.^{1,2}

For studying the dynamics of complex systems, means to determine their total energies and associated forces are required. Empirical force fields were initially developed to characterize the chemical structure and dynamics of macromolecules, including peptides and proteins.³⁻¹⁰ Their primary applications concerned sampling conformations of large molecules, such as proteins in the gas phase¹¹ and in solution.¹² The typical mathematical form of an empirical force field contains bonded and nonbonded terms. The bonded part is

$$\begin{aligned} V_{\text{bond}} &= \sum K_b(r - r_e)^2 \\ V_{\text{angle}} &= \sum K_\theta(\theta - \theta_e)^2 \\ V_{\text{dihe}} &= \sum K_\phi(1 + \cos(n\phi - \delta)) \end{aligned} \tag{1}$$

and is geared towards conformational sampling, spectroscopy or thermodynamics and not, e.g., towards describing chemical reactions for which bonds need to be broken and formed. In Eq. 1 the constants K are the force constants associated with the particular type of interaction, r_e and θ_e are equilibrium values, n is the periodicity of the dihedral and δ is the phase which determines the location of the maximum. The sums run over all respective

terms. Nonbonded interactions include electrostatic and van der Waals terms

$$\begin{aligned}
 V_{\text{elstat}} &= \frac{1}{4\pi\epsilon_0} \sum \frac{q_i q_j}{r_{ij}} \\
 V_{\text{vdW}} &= \sum \epsilon_{ij} \left[\left(\frac{R_{\text{min},ij}}{r_{ij}} \right)^{12} - 2 \left(\frac{R_{\text{min},ij}}{r_{ij}} \right)^6 \right]
 \end{aligned}
 \tag{2}$$

where the sums run over all nonbonded atom pairs. q_i and q_j are the partial charges of the atoms i and j , and ϵ_0 is the vacuum dielectric constant. For the van der Waals terms, the potential energy is expressed as a Lennard-Jones potential with well depth $\epsilon_{ij} = \sqrt{\epsilon_i \epsilon_j}$ and range $R_{\text{min},ij} = (R_{\text{min},i} + R_{\text{min},j})/2$ at the Lennard-Jones minimum, according to standard mixing rules.¹³ This interaction captures long-range dispersion ($\propto -R^{-6}$) and exchange repulsion ($\propto R^{-12}$) where the power of the latter is chosen for convenience. The combination of Eqs. 1 and 2 constitutes a minimal model for an empirical force field.

One of the desirable features of an empirical force field is that it is a computationally efficient model that can be improved in various ways based on physical principles such as to allow direct comparison with experiment and eventually provide a basis for interpretation. Forces can be evaluated analytically which is an advantage for molecular dynamics (MD) simulations. For example, harmonic bonds can be replaced by Morse oscillators which are either useful to investigate chemical reactions or accurate vibrational spectroscopy. These two aspects are of particular relevance to the present work.

Using point charges for the electrostatic interactions can be considered as the zero-order expansion of a more comprehensive multipolar expansion which considerably improves the description of the charge distribution around molecular building blocks.¹⁴⁻¹⁹ In addition, the standard form of an empirical force field can be complemented by including further terms such as polarization.²⁰ The extensibility and specific ways to improve the quality of an empirical force field make it an ideal starting point for using them in increasingly realistic

simulations of molecular materials at an atomistic level.

Following chemical reactions - i.e. the breaking and formation of chemical bonds - as a function of time lies at the heart of chemistry. However, the most obvious and direct route, evaluating the electronic structure along a molecular dynamics (MD) trajectory or time-dependent quantum dynamics simulation, is often impractical for several reasons. For one, evaluating the total energy and forces by solving the electronic Schrödinger equation is computationally prohibitive. This precludes using high-level quantum chemistry methods and/or sufficiently large basis sets for running a statistically significant number of independent trajectories. For converged observables, averages over initial conditions need to be computed. Also, some electronic structure calculations can be affected by systematic error, such as basis set superposition errors, and convergence of the Hartree-Fock wavefunction to the desired state can be challenging. This can occur for systems containing metal atoms, higher excited states or systems with challenging electronic structure.

In the present perspective several improvements to empirical energy functions and their application that have been pursued in the more recent past will be highlighted. The applications focus on vibrational spectroscopy, reactive dynamics and thermodynamic properties which provide a wide range of challenging problems for understanding and interpreting physico-chemical experiments at a molecular level.

Methodological Background

Both, bonded and non-bonded parts of an empirical force field can be systematically improved. An instructive example are recent efforts to correctly describe condensed-phase and spectroscopic properties of liquid water. Building on the realization that multipolar inter-

actions are required,^{17,21–26} the TL4P water model was developed.²⁷ TL4P is a rigid water model with the atoms fixed to the experimental liquid phase geometry. The electrostatic interactions are described by three point charges (one on each hydrogen atom and one on a massless point M that is displaced from the oxygen atom) and a Gaussian inducible dipole. The van der Waals interactions are represented as a Buckingham potential acting between oxygen atoms. With this model, parametrized to reference density functional theory calculations, a wide range of bulk properties could be described reliably compared with experiment (see Table 7 of Ref.²⁷).

When using TL4P for computing the low-frequency part of the infrared and Raman spectra of liquid water it was found that the shapes of the spectral features did not compare well with experiment.²⁸ Based on earlier work it was decided to augment the TL4P water model with some amount of charge transfer along the O–HO intramolecular hydrogen bond and to include anisotropic polarizability.²⁹ The parameters were again determined from reference DFT calculations and both, bulk properties and the optical spectra were computed. With these modifications, the bulk properties were in equally good agreement with experiment as for the original TL4P model²⁷ whereas the relative intensities and peak positions for both, infrared and Raman, spectra compared well with experiment. In this way, a physically motivated, and computationally efficient model for water was developed by refinement, largely guided by comparison with experiment.

Following very different strategies, other successful force fields for water have been developed in the recent past. One of them is the AMOEBA model which builds explicitly on atomic multipoles.^{22,23} Another strategy is followed in the E3B model which is based on adding explicit three-body terms, akin to a many body expansion.³⁰ Similarly, the HBB (Huang, Braams, Bowman) force field also uses a many-body expansion.³¹ As a more recently developed force field, the RexPoN force field is entirely based on reference electronic structure

calculations without empirical data.³² Finally, the most comprehensive water force field in various phases is probably the MB-Pol model which also builds on multipolar interactions and many-body polarization.³³

Multipolar and Polarizable Force Fields

Multipolar interactions have been considered early on in molecular recognition.³⁴ Different from the spherically symmetric field around a point charge, atomic multipoles can capture anisotropic interactions. A typical example is carbon monoxide which can not be realistically modelled with two atom-centered point charges located each of the two atoms (Eq. 2) because the total charge ($Q = 0$) and the total molecular dipole $\mu = 0.048 ea_0$ lead to two partial charges close to zero but with opposite sign. In order to describe the substantial molecular quadrupole moment^{35–37} ($\Theta = -1.58 ea_0^2$) either a third interaction site midway the two atoms can be included³⁸ or the two atoms are described by a distributed multipole expansion.^{14,21,39,40}

More generally, the electrostatic potential (ESP) around a molecule can be represented as a superposition of point charges (PC) and higher multipole (MTP) moments. Capturing strongly anisotropic features—e.g., lone pairs, hydrogen bonding, π -electron density or sigma holes (halogens)^{41–43} requires schemes beyond point charge representations. The ESP $\Phi(\mathbf{r})$ is related to the charge distribution $\rho(\mathbf{r})$ through

$$4\pi\epsilon_0\Phi(\mathbf{r}) = \int d\mathbf{r}' \frac{\rho(\mathbf{r}')}{|\mathbf{r} - \mathbf{r}'|} = \sum_{l=0}^{\infty} \sum_{m=-l}^l \frac{Q_{lm}}{r^{l+1}} \sqrt{\frac{4\pi}{2l+1}} Y_{lm}(\theta, \phi), \quad (3)$$

where \mathbf{r} and \mathbf{r}' are spatial variables. For the second equation $1/|\mathbf{r} - \mathbf{r}'|$ was expanded in powers of $r'/r < 1$ ⁴⁴ to represent the ESP as a sum over spherical harmonics $Y_{lm}(\theta, \phi)$ from

which the spherical MTP moments Q_{lm} are defined by

$$Q_{lm} = \int d\mathbf{r}' \rho(\mathbf{r}') (r')^l \sqrt{\frac{4\pi}{2l+1}} Y_{lm}^*(\theta', \phi') \quad (4)$$

These can be determined from the density by integration. This provides a compact atom-based representation of the ESP around a molecule.

Alternatively, multipoles of a given order can be represented by distributed point charges as is done in the distributed charge model (DCM).^{18,19} Such a model replaces the evaluation of multipole-multipole interactions at the expense of using a larger number of terms. Reducing the number of interaction sites can be accomplished by finding the smallest number of point charges to accurately represent the ESP using differential evolution.¹⁹

Reactive Force Fields

The design of reactive force fields has followed different routes. Early work by Penney⁴⁵ and Pauling⁴⁶ related bond order, bond length, and bond strength. The finding that bond order and bond length follow a near linear relation⁴⁶ and a log-log plot of dissociation energies versus bond order is also almost linear was used to develop “bond energy bond order” (BEBO) potentials.⁴⁷ One of the essential assumptions underlying this approach is that - at least for hydrogen-atom transfer reactions - the sum of the bond orders of the broken bond, n_1 , and of the newly formed bond, n_2 , fulfills $n_1 + n_2 = 1$. In other words: ”At all stages of the reaction the formation of the second bond must be ’paying for’ the breaking of the first bond”.⁴⁷

An extension of the concept underlying BEBO is ReaxFF.⁴⁸ Here, nonbonded terms are included from the beginning and the dissociation and reaction curves are derived from fitting to electronic structure calculations.^{48,49} Central to ReaxFF is that the bond order is related to

the distance between two atoms. As an example, for two carbon atoms there can be anything between “no bond” (bond order = 0) to a triple bond. In ReaxFF the total energy consists of a sum of individual terms such as E_{bond} , a correction for over-coordination, a penalty term E_{over} for under-coordinated atoms reflecting resonance energies between π -electrons, a conjugation energy and others. Contrary to empirical force fields,⁷⁻⁹ ReaxFF does not build on the concept of atom types. While the functional form of ReaxFF is universal, its application to concrete problems always involves more or less extensive fitting to reference calculations.⁵⁰

Chemical reactivity can be encapsulated in a natural fashion within the framework of valence bond theory. For ionic bond cleavage $AB \rightarrow A^- + B^+$, three chemically relevant states are considered within empirical valence bond (EVB)⁵¹ theory: $\psi_1 = AB$, $\psi_2 = A^-B^+$, and $\psi_3 = A^+B^-$. If A is more electronegative than B (i.e. formation B^- is unlikely in the presence of A), resonance structure ψ_3 is largely irrelevant and the process can be described by ψ_1 and ψ_2 alone. For a more general chemical reaction, one must choose, “..on the basis of experience and intuition, a set of bonding arrangements or “resonance structures”[..]” as was noted in the original EVB publication.⁵¹ The choice of the states in EVB is not always obvious *a priori* but may also need to be based, e.g., on the requirement to best reproduce the reference electronic structure calculations.⁵²

The total n -state EVB Hamiltonian H_{nn} contains diagonal terms (force fields for each of the n states) and the coupling between them (H_{ij}). Representation and parametrization of the off-diagonal terms has been a source of considerable discussion,⁵³⁻⁵⁵ in particular the assumption that upon transfer of the reaction from the gas phase to the solution phase these elements do not change significantly.⁵⁶ Applications of EVB include enzymatic reactions (for which it was originally developed⁵⁷), proton transfer processes, and the autodissociation of water.⁵⁸ More recently, this has been extended to other types of reactions, including bimolecular reactions^{59,60} or the association and dissociation of CH_3 from diamond surfaces.⁶¹

Furthermore, several extensions have been suggested to the original EVB method allowing its application to a wider class of problems.⁶²⁻⁶⁴

Time resolved experiments have contributed considerably to our understanding of chemical reactivity over the past 3 decades. Short laser pulses (“femtochemistry”) allow to follow chemical transformations on time scales relevant to the actual chemical step (bond breaking or bond formation). Typical examples are the time resolved studies of ligand (re)binding in myoglobin (Mb)⁶⁵⁻⁶⁸ or vibrationally induced reactivity.⁶⁹⁻⁷¹ This prompted the development of time-based reactive MD^{72,73} whereby a chemical reaction is followed in time which is the natural progression coordinate in such an experiment. For the example of two states (“R” and “P”) the two PESs are mixed according to $V_{\text{eff}}(\vec{x}) = f(t)V_{\text{R}}(\vec{x}) + (1 - f(t))V_{\text{P}}(\vec{x})$ where $f(t)$ is a sigmoid switching function which changes from 1 to 0 between $t = -t_s/2$ and $t = t_s/2$. At the beginning of the mixing the system is fully in the R-state ($f(t = -t_s/2) = 1$), while at the end it is fully in the P-state ($f(t > t_s/2) = 0$). Here, the only free variable is the switching time t_s . The algorithm of ARMD is schematically shown for a collinear atom transfer reaction in Figure 1a.

During the mixing the system is propagated under a time-dependent Hamiltonian which does not strictly conserve total energy.^{74,75} The magnitude of this effect can be shown to scale with $1/m$ where m is the reduced mass involved in the reaction⁷⁵ which is inconsequential for heavy systems such as NO rebinding to Mb but affects the dynamics in the product channel for proton transfer processes. This led to the development of multi state adiabatic reactive MD (MS-ARMD) which mixes the PESs with energy dependent weights and strictly conserves energy.⁷⁵

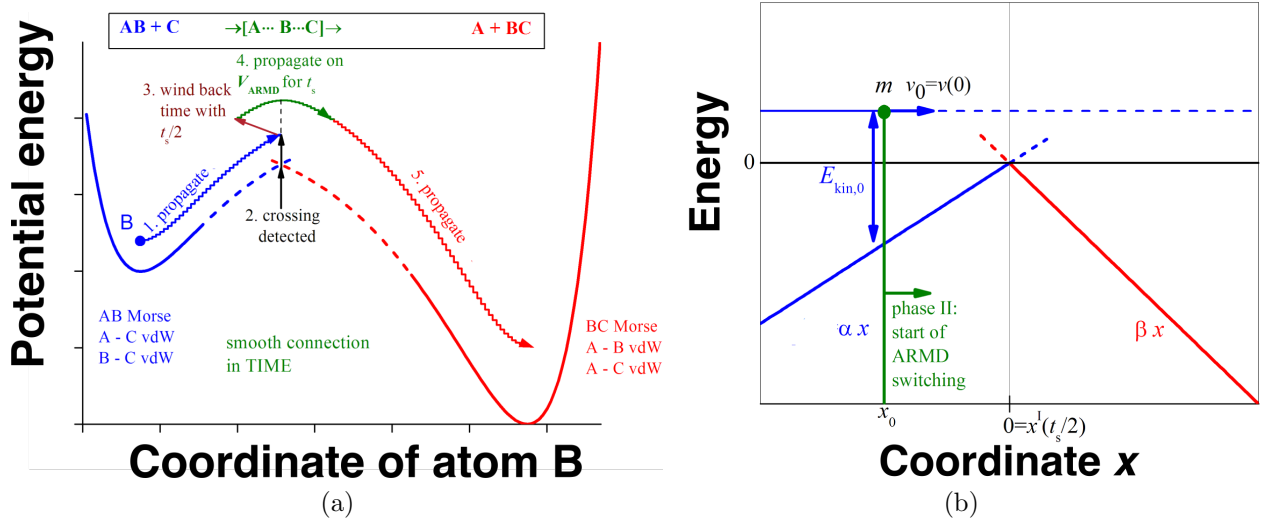


Figure 1: a) Schematic illustration of the ARMD method for a collinear reaction, where atom B is transferred from donor atom A to acceptor atom C. During crossing the surfaces are switched in time and the Morse bond is replaced by van der Waals (vdW) interactions and vice versa. b) Simple model for estimating energy violation in ARMD simulations. The system with mass m approaches from the left on PES $V_R(x) = \alpha x$ (phase I). At time $t = 0$ it is at x_0 with velocity v_0 and kinetic energy $E_{\text{kin},0}$. After crossing is detected at $x = 0$ the time is rewound by $t_s/2$ and the dynamics is re-simulated while $V_R(x)$ is being switched to $V_P(x) = \beta x$ in t_s (phase II).

In MS-ARMD the PESs are mixed in energy-space according to

$$V_{\text{MS-ARMD}}(\vec{x}) = \sum_{i=1}^n w_i(\vec{x}) V_i(\vec{x}) \quad (5)$$

The weights (see Figure 2) $w_i(\vec{x})$ are obtained by renormalizing the raw weights $w_{i,0}(\vec{x})$

$$w_i(\vec{x}) = \frac{w_{i,0}(\vec{x})}{\sum_{i=1}^n w_{i,0}(\vec{x})} \quad \text{where} \quad w_{i,0}(\vec{x}) = \exp\left(-\frac{(V_i(\vec{x}) - V_{\min}(\vec{x}))}{\Delta V}\right) \quad (6)$$

where $V_{\min}(\vec{x})$ is the minimal energy for a given configuration \vec{x} and ΔV is a parameter. The raw weights (Eq. 6) depend exponentially on the energy difference between surface i and the minimum energy surface $V_{\min}(\vec{x})$ over a characteristic energy scale ΔV (switching parameter). Only those surfaces will have significant weights, whose energy is within a few times of ΔV from the lowest energy surface $V_{\min}(\vec{x})$ for instantaneous configuration \vec{x} . The

performance of MS-ARMD is demonstrated for crossings of 1D and 2D surfaces in Figure 2. Finally, ARMD with energy-dependent weights mixes the different PESs by using Gaus-

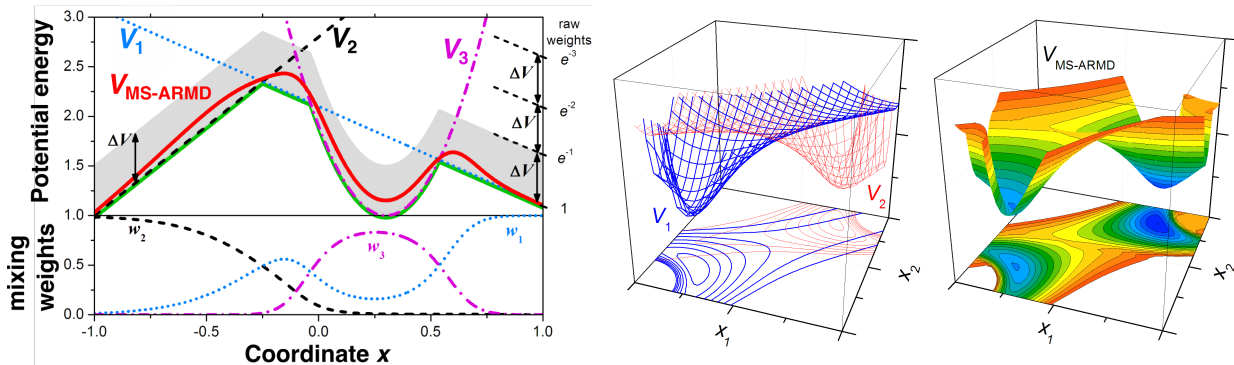


Figure 2: The MS-ARMD switching method applied in one and two dimensions to 3 and 2 surfaces ($V_{1,2,3}$). The effective surface is ($V_{\text{MS-ARMD}}$) always close to the lowest-energy surface (V_{min}), except for regions where other surfaces are within a few times ΔV (here = 0.5) in energy. Here, the algorithm switches smoothly among them by varying their weights ($w_{1,2,3}$; lower left panel)

sian and polynomial functions (GAPOs) in the neighborhood of crossing points between the states. The parameters of these GAPOs need to be determined through fitting to reference data (e.g. from a calculation along the intrinsic reaction coordinate (IRC)). This step is the most demanding part in MS-ARMD.⁷⁵ A smooth global surface is obtained everywhere, even for energies where more than two surfaces approach one another. Because the mixed PES $V_{\text{MS-ARMD}}(\vec{x})$ depends on the energies of the different states through the weights w_i which in turn are analytical functions of the coordinates \vec{x} , the derivatives can be readily determined which leads to energy conservation in MD simulations.

A recent extension⁷⁶ of MS-ARMD is its combination with VALBOND, a force field that allows to describe the geometries and dynamics of metal complexes.⁷⁷⁻⁷⁹ Here, the formulation is reminiscent of EVB whereby the diagonal terms are VALBOND descriptions of the states involved and the off-diagonal elements describe the orbital overlap. Furthermore, MS-ARMD can also be combined with molecular mechanics with proton transfer (MMPT)⁸⁰ to follow proton transfer in the gas- and condensed phase.⁸¹⁻⁸⁴

Applications in Vibrational Spectroscopy

Vibrational spectroscopy is a sensitive tool for quantitatively characterizing the structure of and the structural dynamics around a solute embedded in an environment.⁸⁵ Such studies can also provide important insight into the dynamical coupling between the solute and the solvent. One example is the possibility to infer ligand binding strengths from infrared spectroscopic measurements.⁸⁶ A quantitative study for benzonitrile in lysozyme has been carried out recently using atomistic simulations with non-conventional force fields.⁸⁷

Refined multipolar force fields also allow quantitative comparisons with experiments and their interpretation. One of the noticeable examples is the infrared spectrum of photodissociated carbon monoxide (CO) in myoglobin (Mb).⁸⁸ The strong (43 MV/cm⁸⁹) inhomogeneous electric field in the heme pocket leads to characteristic shifting and splitting of the spectral lines due to the Stark effect. Several attempts were made⁹⁰⁻⁹² to correctly interpret the experimental infrared spectrum using computational methods. Although some of them were capable of correctly modelling the width of the spectrum they usually were unable to find the characteristic splitting of the CO spectrum (i.e., $\approx 10 \text{ cm}^{-1}$). A first successful attempt used a fluctuating point-charge model²¹ based on an earlier three-point model for CO.³⁸ This was later generalized to a rigorous fluctuating MTP model which reproduced most features of the spectrum known from experiments.⁴⁰ In particular, the splitting, width and relative intensities of the computed spectrum agreed favourably with the experimentally known properties. Based on this it was then also possible to assign the two spectroscopic signatures to distinct conformational substates. Those agreed with results from more indirect (based on mutations in the active site)⁹³ or more difficult-to-converge mixed QM/MM simulations from MD simulations.⁹⁴

Understanding structural, spectroscopic and dynamical properties of water in its different phases provides a rich variety for developing and improving special-purpose, tailored and physics-based force fields. Among the most successful for spectroscopic applications are MB-pol³³ and WHBB.⁹⁵ Other, similarly successful models, include the explicit 3-body (E3B) parametrization,³⁰ the (i)AMOEBA family of force fields,^{22,23} the TLnP family²⁷ and a recent modification of it.²⁹

The ManyBody-polarizable (MB-pol) model is based on two- and three-body water interactions calculated at the CCSD(T) level of theory. It is entirely developed from first-principles.^{33,96} MB-pol explicitly treats the one-body (monomer distortion energy) term and the short-ranged two- and three-body terms akin to a polarizable potential supplemented by short-range two- and three-body terms that effectively represent quantum-mechanical interactions arising from the overlap of the monomer electron densities. Specifically, at all separations, the total MB-pol two-body term includes (damped) dispersion forces derived from ab initio computed asymptotic expansions of the dispersion energy along with electrostatic contributions due to the interactions between the molecular permanent and induced moments. Similarly, the MB-pol three-body term includes a three-body polarization term at all separations, which is supplemented by a short-range 4th-degree permutationally invariant polynomial that effectively corrects for the deficiencies of a purely classical representation of the three-body interactions in regions where the electron densities of the three monomers overlap. This short-range three-body contribution is smoothly switched off once the oxygen-oxygen separation between any water molecule and the other two water molecules of a trimer reaches a value of 4.5 . In MB-pol, all induced interactions are described through many-body polarization. MB-pol thus contains many-body effects at all monomer separations as well as at all orders, in an explicit way up to the third order and in a mean-field fashion at all higher orders. Using MD simulations the computed infrared and Raman spectra for liquid water

can be realistically modelled. Finally, molecular dynamics (MB-MD) simulations carried out with MB-pol describe the infrared (IR) and Raman spectra of liquid water well compared with experiments.⁹⁷

The WHBB model⁹⁵ is the sum of monomer, 2-body, and 3-body, full-dimensional potentials, with the option of including 4 and higher-body interactions from other polarizable potentials. The monomer PES is spectroscopically accurate and the 2- and 3-body potentials are mathematical fits to tens of thousand of ab initio electronic energies (CCSD(T)/aug-cc-pVTZ (aVTZ) and MP2/ aVTZ energies) using permutationally invariant polynomials.⁹⁸ The WHBB model has been applied to the infrared spectroscopy of liquid water and showed to perform well compared with experiment.⁹⁹

Multipolar force fields have recently been used for a number of 1d- and 2d-spectroscopy studies including N-methylacetamide,¹⁰⁰ fluoro-acetonitrile,¹⁰¹ cyanide,¹⁰² insulin in water,¹⁰³ and azide in gas phase and in water.¹⁰⁴ As an example for using such simulations in a concrete context, the 1d-infrared spectroscopy of wild type insulin monomer (WT-MO, chains A and B, see Figure 3) and dimer (WT-DI, chains A to D) in solution is discussed here. For this, the X-ray crystal structure of WT insulin dimer resolved at 1.5 Å (protein data bank (PDB^{105,106}) code: 4INS)¹⁰⁷ were solvated in a cubic box (75^3 Å³) of TIP3P¹⁰⁸ water molecules. For all molecular dynamics (MD) simulations the CHARMM¹⁰⁹ package together with the CHARMM36¹¹⁰ force fields was used. The systems were minimized and equilibrated for 20 ps in the *NVT* ensemble. Production runs, 1 ns in length, were carried out in the *NPT* ensemble, with coordinates saved every 10 fs for subsequent analysis. A velocity Verlet¹¹¹ integrator and Nosé-Hoover thermostat^{112,113} was employed in the *NVT* simulations. For the *NPT* simulations, an Andersen and Nosé-Hoover constant pressure and temperature algorithm¹¹³⁻¹¹⁵ was used together with a leapfrog integrator.¹¹⁶

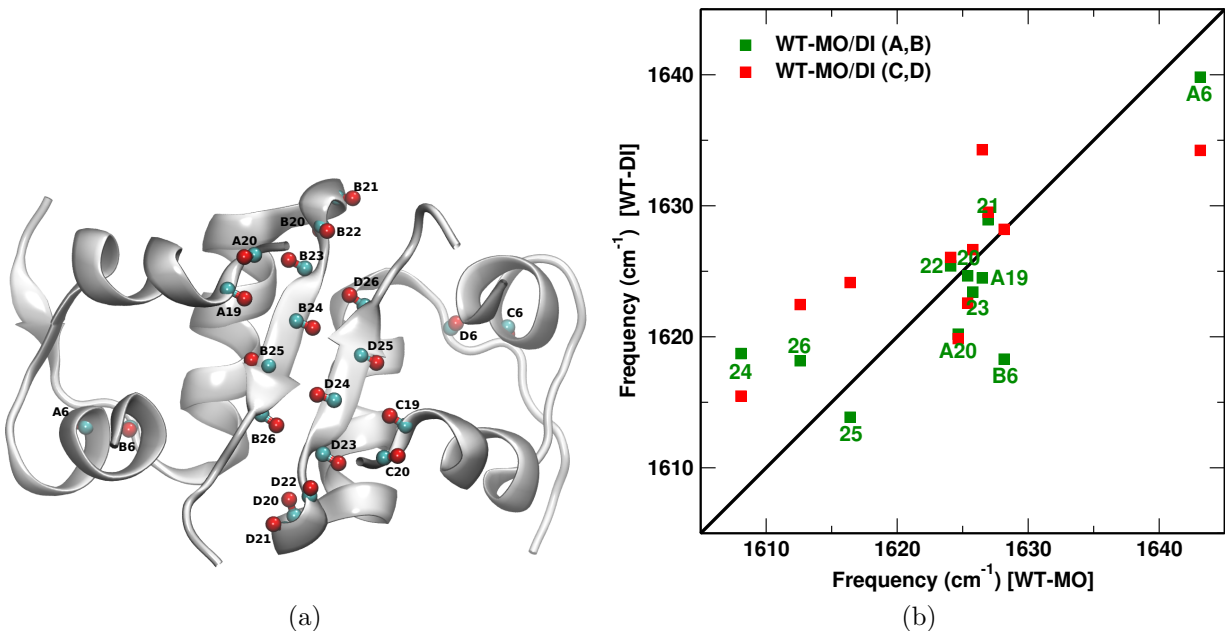


Figure 3: a) Structure of the WT insulin dimer with the CO labels considered specifically. b) Comparison between the maxima of the frequency distribution for WT-MO and WT-DI. Residues of chain A/B and C/D are shown in green and red, respectively.

Time-ordered snapshots were extracted from the MD simulation every 10 fs and then the anharmonic frequencies were computed. For this purpose, one-dimensional potential energy curves were calculated along the $-CO$ normal modes for each snapshot. The anharmonic transition frequencies ($v = 0 \rightarrow 1$) were then calculated by solving the 1D time-independent Schrödinger equation to obtain the frequency trajectory. Figure 3B compares the maximum of the frequency distribution for 10^5 snapshots between monomer and dimer for several residues (6, 19, and 20 from chains A/C and 6, and 19-26 from chains B/D) for the WT protein. Residues 24 to 26 of the B/D chains are involved in hydrogen bonding at the dimerization interface. As is shown in Figure 3B, the maximum frequencies for residues 24 and 26 of chain B/D are both blue shifted when going from the monomer to the dimer while for residue 25B a small red shift is observed and clearly blue shifted for residue 25D. This is also consistent with previous results¹⁰³ which showed that the IR spectra of the symmetry-related pairs of chain B/D do not superimpose. This also suggests that the structural dynamics and spectroscopy of the CO probes involved in the protein-protein contact (24-26 B/D) repre-

sent characteristic changes and this feature can be used to distinguish the monomeric from dimeric insulin in solution.

As a second example, the influence of the scanning direction in determining the local frequency is explored. For this, simulations of N-methyl acetamide (NMA) were carried out in which the entire NMA molecule was treated with MTP electrostatics.^{25,26,100,117} For the bonded terms, a reproducing kernel Hilbert space (RKHS-)based representation of the PES has been constructed for the amide-I stretch (CONH) fragment. For convenience, this was based on PBEPBE/cc-pVTZ reference calculations although the approach can also be applied to reference data calculated at much higher levels of theory. In the simulations, the electrostatic interactions are treated using Particle-Mesh Ewald¹¹⁸ (PME) with grid size spacing of 1 Å, characteristic reciprocal length $\kappa = 0.32 \text{ \AA}^{-1}$, and interpolation order 4. All bonds involving hydrogen atoms were constrained using SHAKE¹¹⁹ except for the NH bond in amide-I mode .

To construct the RKHS PES (for details on RKHS, see^{120,121}), the NMA structure was optimized first and then the normal modes are calculated by fixing all hydrogen atoms of the methyl groups. Next, gas phase PBEPBE/cc-pVTZ energies and forces were calculated using Gaussian09 software¹²² for 2400 structures sampled randomly along the 12 normal modes. In order to describe the PES for the NMA fragment (X(CONH)Y where “X” and “Y” are the two methyl groups as united atoms), a multidimensional reproducing kernel based function is considered which is the sum of 15 four-body interactions (${}^6C_4 = 15$ where nC_k is the binomial coefficient). Each of the four-body interactions is represented by a 6-dimensional tensor product kernel for 6 radial dimensions (the interatomic distances in a tetra-atomic systems). A reciprocal power decay kernel of type ($n = 3, m = 0$) was used for all the bond distances.^{120,121} The kernel coefficients were calculated using least square fitting. Finally RKHS PES has been constructed for the Amide-I stretch mode. This RKHS PES describes

all relevant bonded terms for the CONH motif and also the bonded interaction in $\text{H}_3\text{C-C}$ and $\text{H}_3\text{C-N}$. The harmonic frequency calculated for the Amide-I stretch from the RKHS PES compares well with the one obtained from the DFT calculations (1696 vs. 1698 cm^{-1}) which serves as a validation of the present approach.

To simulate the dynamics of NMA, the RKHS-based representation for the bonded terms is implemented in CHARMM and supplemented with conventional force field parameters to describe the interactions between the methyl hydrogen atoms and all other atoms. The harmonic frequency of the amide-I stretch for NMA is at 1714 cm^{-1} , slightly higher than that computed using the stand-alone RKHS PES (1696 cm^{-1}) from above. This is due to coupling between the CONH motif and the rest of the NMA molecule. Next, MD simulations are run for the solvated system and the 1-dimensional potential energy is scanned along two different directions: the CO and the CONH directions, see Figure 5, to investigate the differences depending on the approach chosen.

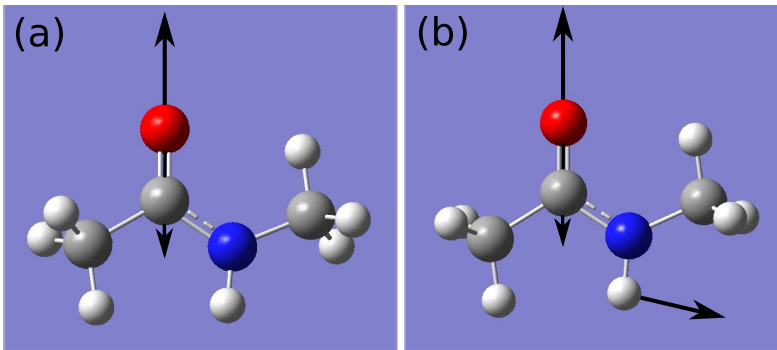


Figure 4: Displacement vector for two different scanning to construct an 1D potential. (a) Distortion along the CO stretching and (b) movement along the CONH stretching.

The anharmonic frequencies for the fundamental and overtones of a particular mode and corresponding eigen functions can be calculated by solving 1D Schrödinger equation using a discrete variable representation (DVR) approach.¹²³ For the amide-I mode in NMA - which can also be applied to the protein backbone, see above - two different schemes are

followed: (a) scanning along the CO stretch, and (b) displacing the CONH group along the amide-I normal mode (see Figure 4). The potential energies are again represented by a 1d-reproducing kernel and the Schrödinger equation is then solved using a DVR approach for $-\infty < r < \infty$, where r is the displacement from the equilibrium geometry. The anharmonic stretching frequencies in the gas phase are computed as 1671 and 1695 cm^{-1} using the potential obtained following schemes (a) and (b), respectively. The reduced mass is 1 amu for both cases, since unnormalized displacement coordinates are used to distort the molecule along the normal modes.

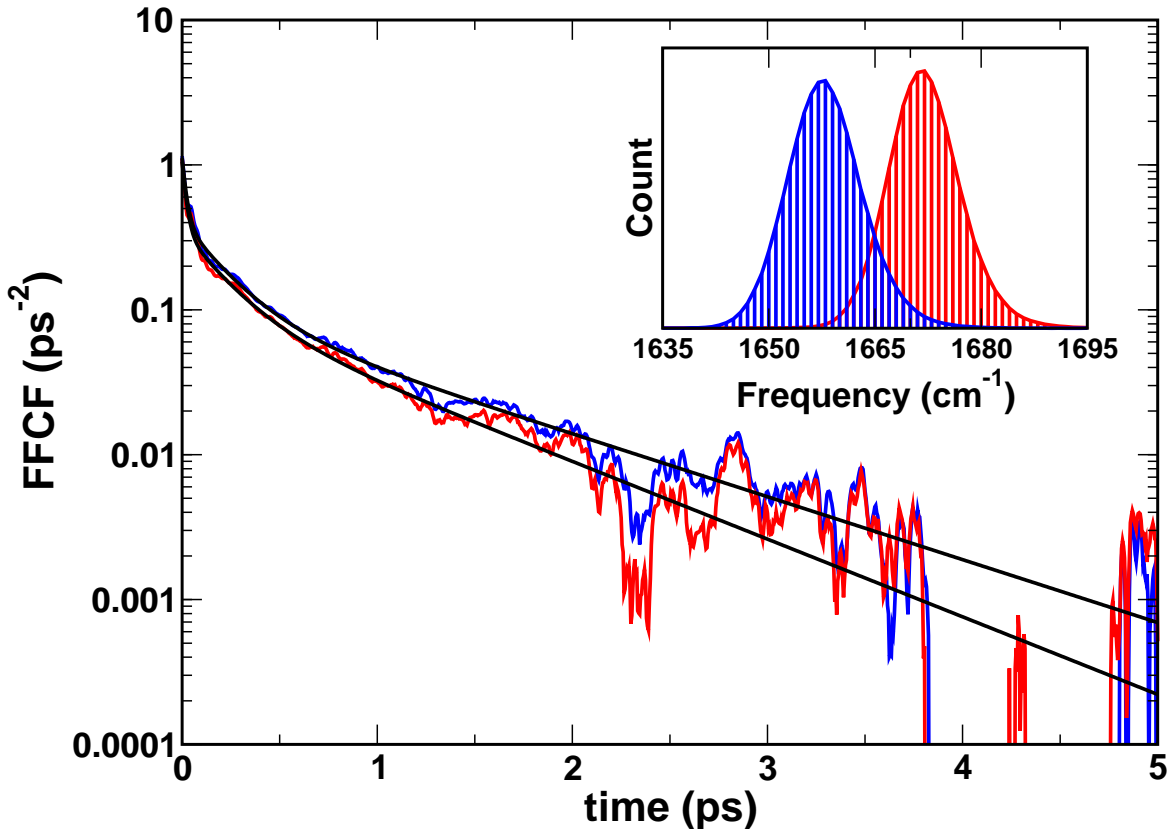


Figure 5: Frequency fluctuation correlation functions (FFCF) of NMA in water with anharmonic frequency calculated via scanning along CONH mode (red) and CO stretching mode (blue) using multipolar force fields and gas phase RKHS potential of NMA described above. The black lines refer to the tri-exponential fit to the FFCF. Inset shows the corresponding frequency distributions.

Using the RKHS based PES described above, a 4 ns trajectory of solvated NMA (30^3 \AA^3

TIP3P water¹⁰⁸) in the NVE ensemble was run following 20 ps of heating and 1.2 ns of equilibration at 300 K. The trajectory was saved every 5 fs and the anharmonic frequencies were determined from scanning the RKHS-potential along the CO and the CONH directions (see Figure 4) for 8×10^5 snapshots using MTP electrostatics. The MTPs mainly account for the NMA-water electrostatic interactions while the gas phase RKHS potential accurately represents the amide-I mode within NMA. Figure 5 shows the decay of the frequency fluctuation correlation function (FFCF) and frequency distribution (see inset in Figure 5) for NMA in water with anharmonic frequency calculated via scanning along the two directions. The average frequencies for scanning along the CO (a) and CONH mode (b) of NMA in water are at 1657 cm^{-1} and 1671 cm^{-1} , respectively. A tri-exponential fit to the frequency fluctuation correlation functions yields three timescales which are close to one another from approaches (a) and (b) and compare quite well with experiment^{124,125} and previous simulations,¹⁰⁰ see Table 1.

Table 1: The FFCF decay times and their amplitudes for scanning along the CO and CONH normal modes for solvated NMA obtained from a tri-exponential fit, see Figure 5. The frequency calculations used the RKHS PES and MTP electrostatics. For comparison, vibrational decay times from experiment¹²⁴ and simulations¹²⁵ are also given.

Method	a_1 [ps ⁻²]	t_1 [ps]	a_2 [ps ⁻²]	t_2 [ps]	a_3 [ps ⁻²]	t_3 [ps]
CO scan	0.71	0.021	0.302	0.208	0.103	1.0
CONH scan	0.70	0.020	0.25	0.20	0.106	0.81
sim. ¹²⁵		0.06				0.66
exp. ¹²⁴		(0.05-0.1)				1.6
exp. ¹²⁵		0.01				1.0

As a final example for a spectroscopic application, a recent model for azide in gas phase and in solution is discussed. The bonded terms were again based on RKHS which exactly reproduces the energies from the reference *ab initio* calculations. For N_3^- , a 3-dimensional PES based in multi reference CI (MRCI) calculations was represented as an RKHS and quantum bound states were determined.¹⁰⁴ The agreement with gas phase experiments was found to be good, typically within $\sim 10 \text{ cm}^{-1}$. Simulations in solution provided the correct blue shift,

consistent with experiment. This opens now the possibility to use the new parametrization of N_3^- for simulations of proteins in solution and to determine the site-specific dynamics depending on the position of the label.

Applications in Reaction Dynamics

The investigation of chemical reactions using atomistic simulations dates back to the 60s when the first studies of the $H+H_2$ reactions were carried out.¹²⁶ One unexpected finding was that such quasi-classical trajectory (QCT) simulations agree quite well with quantum simulations¹²⁷ despite the fact that the $H+H_2$ system is particularly susceptible to quantum effects including zero point energy and tunneling. In the following, QCT simulations became an established way to investigate small- and large-molecule reactive processes.

Small-Molecule Reactions Involving Tri- and Tetra-Atomics

The field of small molecule reactions was heavily driven by the advent of refined experimental techniques, such as molecular beam studies or photodissociation spectroscopy which provide energy-, state- and conformationally-resolved information about reactive molecular collisions. Initially, empirical energy functions, such as the London-Eyring-Polanyi-Sato (LEPS) surface,¹²⁸⁻¹³⁰ were used to carry out QCT simulations. Once electronic structure calculations became sufficiently accurate and the configurational space could be covered by computing energies for many geometries, such empirical PESs were largely superseded. The primary problem then shifted to representing the computed points such that the total potential energy can be evaluated with comparable accuracy as the underlying quantum chemical calculations.

For triatomic molecules a convenient representation was one that used an expansion into Legendre polynomials $P_\lambda(\cos \theta)$ and corresponding radial strength functions $V_\lambda(R, r)$, i.e. $V(R, r, \theta) = \sum_{\lambda=0}^{\lambda_{\max}} V_\lambda(R, r) P_\lambda(\cos \theta)$. Such expansions have been particularly useful for studying van der Waals complexes.^{131–134} Such representations have been used either together with explicit fits to experimental data, or by fitting them to reference electronic structure calculations. An alternative is to separate the total interaction energy into long- and short-range parts and to represent them separately. Often, the long range part in such complexes can be described very accurately by resorting to classical electrostatics based on atomic and molecular multipoles and polarizabilities and hyperpolarizabilities.^{135,136}

An alternative is an expansion into permutationally invariant polynomials (PIPs)⁹⁸ which has, for example, been applied to N_4 for studying reactive collisions for $N_2 + N_2 \rightarrow N_2 + 2N$ and $N_2 + N_2 \rightarrow 4N$.¹³⁷ PIPs employ a basis of exponential or Morse-type functions to expand the PES and fit products of such basis functions to the reference data. The permutational symmetry of chemically identical atoms is preserved in such an approach. Similarly, a study of N_4^+ using an RKHS representation also incorporated permutational invariance explicitly.¹³⁸

Another method is a representation based on a Reproducing Kernel Hilbert Space (RKHS).^{120,121,139} Such an approach *exactly* reproduces the input data which are usually results from electronic structure calculations on a predefined grid. One of the advantageous features of an RKHS is that the physical long range decay for a radial coordinate $\rightarrow \infty$ can be encoded in the functional form of the kernel. Such RKHS-based representations have been used for entire PESs¹⁴⁰ or in a QM/MM-type approach to treat part of an extended system with higher accuracy.^{141–143}

Recently, RKHS-based reactive PESs have been successfully used for a range of atom+diatom reactions. For these systems the focus was primarily on thermal reaction rates, final state

distributions and vibrational relaxation times which are properties of particular interest to hypersonics and atmospheric re-entry.^{144–146} Reference data for the systems of interest ([NOO], i.e. N+O₂ and O+NO; [NNO], and [CNO]) can be determined at high levels of theory (MRCI) with good-quality basis sets (aug-cc-pVTZ or larger).^{140,147–149} A typical PES for one electronic state is based on 10⁴ energies and the RKHS-interpolated surfaces reproduce the reference data to within much better than chemical accuracy, typically within a few cm⁻¹. Extensive QCT simulations on these PESs now provide a comprehensive and consistent set of thermal rates and vibrational relaxation times for the most relevant systems involved in hypersonics.¹⁵⁰

Larger Molecules and Proteins

For larger molecules in the gas phase, MS-ARMD has also been used together with established empirical force fields. This has been applied to the study of specific reaction channels such as proton transfer within H₂SO₄ or photodissociation of H₂SO₄ → H₂O + SO₃¹⁵¹ and other atmospherically relevant molecules following vibrational excitation of the OH stretch,^{152,153} the Claisen rearrangement reaction¹⁵⁴ or to investigate Diels-Alder reactions.¹⁵⁵ Such studies provide molecular-level details into the reaction mechanisms and relevant coordinates driving the reaction based on dynamics studies which goes beyond scanning and relaxing the energy function along a minimum energy path. As an example, for the Diels-Alder reaction between 2,3-dibromo-1,3-butadiene and maleic anhydride such reactive dynamics simulations emphasized the important role played by rotations of the two reactants to reach the transition state.¹⁵⁵

Finally, biological systems can also be studied with a combination of RKHS-based PES and an empirical force field.^{142,143} Such studies allowed a structural interpretation of metastable states in MbNO and a molecularly refined understanding of ligand exchange (NO vs. O₂) at

the heme-iron in truncated hemoglobin.

Outlook

Very recent developments in accurate representations of multidimensional potential energy surfaces use generalizations of PIPs¹⁵⁶ or machine learning within the context of kernel ridge regression¹⁵⁷ or neural networks.^{158–160} Common to all these approaches is the fact that they are based on extensive reference data sets. Also, the evaluation time of such representations is computationally considerably more expensive than that of a parametrized empirical function. For the Diels-Alder reaction between 2,3-dibromo-1,3-butadiene and maleic anhydride evaluating the MS-ARMD and NN-based PESs differs by a factor of ~ 200 .¹⁵⁵

As an example for future applications and improvement, the possibility to run MD simulations of molecules with machine learned energy functions and charges in solution is mentioned. PhysNet¹⁶⁰ can be used to train energies, forces and partial charges which yields accurate representations of high-dimensional, reactive PESs.^{155,161,162} As has been noted above, accurate representations of the ESP are required for quantitative investigations of the vibrational spectroscopy in the condensed phase. As PhysNet provides geometry-dependent charges in a natural way, simulations of solutes in aqueous and other environments will benefit greatly from such more realistic representations. This also brings atomistic simulations based on empirical energy functions closer to more rigorous mixed quantum/classical simulations.

It is expected that with the increased performance of computer architecture and the recent advances in machine learning and representing high-dimensional potential energy surfaces, the quality of simulations involving small molecules will further increase. This will bring

experiment, simulation and theory closer together and provide new opportunities to characterize, analyze, and predict molecular properties and processes at an atomic scale. A next step in this endeavour is to transfer and apply this technology to larger systems, including proteins and materials.

Acknowledgments

This work was supported by the Swiss National Science Foundation grants 200021-117810, 200020-188724, the NCCR MUST, the AFOSR, and the University of Basel which is gratefully acknowledged.

References

- (1) Koner, D.; Unke, O. T.; Boe, K.; Bemish, R. J.; Meuwly, M. Exhaustive state-to-state cross sections for reactive molecular collisions from importance sampling simulation and a neural network representation. *J. Chem. Phys.* **2019**, *150*, 211101.
- (2) Grover, M. S.; Torres, E.; Schwartzentruber, T. E. Direct molecular simulation of internal energy relaxation and dissociation in oxygen. **2019**, *31*, 076107.
- (3) Lifson, S.; Warshel, A. Consistent force field for calculations of conformations, vibrational spectra and enthalpies of cycloalkane and n-alkane molecules. *J. Chem. Phys.* **1968**, *49*, 5116–5129.
- (4) Levitt, M.; Lifson, S. Refinement of protein conformations using a macromolecular energy minimization procedure. *J. Mol. Biol.* **1969**, *46*, 269–279.
- (5) Hwang, M. J.; Stockfish, T. P.; Hagler, A. T. Derivation of Class II Force Fields:

2. Derivation and Characterization of a Class II Force Field, CFF93, for the Alkyl Functional Group and Alkane Molecules. *J. Am. Chem. Soc.* **1994**, *116*, 2515–2525.
- (6) Maple, J. R.; Hwang, M. J.; Stockfish, T. P.; Dinur, U.; Waldman, M.; and A. T. Hagler, C. S. E. Derivation of class-II force-fields .1. Methodology and quantum force-field for the alkyl functional group and alkane molecules. *J. Comput. Chem.* **1994**, *15*, 162–182.
- (7) Brooks, B.; Bruccoleri, R.; Olafson, B.; States, D.; Swaminathan, S.; Karplus, M. CHARMM: A program for macromolecular energy, minimization, and dynamics calculations. *J. Comput. Chem.* **1983**, *4*, 18–217.
- (8) Weiner, S. J.; Kollman, P. A.; Case, D. A.; Singh, U.; Ghio, C.; Alagona, G.; Profeta Jr, S.; Weiner, P. A new force-field for molecular mechanical simulation of nucleic-acids and proteins. *J. Am. Chem. Soc.* **1984**, *106*, 765–784.
- (9) Jorgensen, W. L.; Tirado-Rives, J. The OPLS potential functions for proteins - energy minimizations for crystals of cyclic-peptides and crambin. *J. Am. Chem. Soc.* **1988**, *110*, 1657–1666.
- (10) Hermans, J.; Berendsen, H. J. C.; van Gunsteren, W. F.; Postma, J. P. M. A consistent potential for water-protein interactions. *Biopolymers* **1984**, *23*, 1.
- (11) McCammon, J.; Gelin, B.; Karplus, M. Dynamics of folded proteins. *Nature* **1977**, *267*, 585–590.
- (12) Steinbach, P.; Brooks, B. Protein hydration elucidated by molecular dynamics simulation. *Proc. Natl. Acad. Sci. USA* **1993**, *90*, 9135–9139.
- (13) Al-Manthari, M. S.; Al-Wadhahi, M. A.; Vakili-Nezhaad, G. R.; Nasrifar, K. A Systematic Study of Cubic Equations of State with van der Waals Mixing Rules and Different

Combining Rules in Predicting the Densities of LNG and Natural Gas Model Systems. *Intern. J. Thermodyn.* **2019**, *22*, 107–116.

- (14) Stone, A. J. *The Theory of Intermolecular Forces*; Clarendon Press Oxford, 1996; Vol. 32.
- (15) Kramer, C.; Gedeck, P.; Meuwly, M. Atomic multipoles: Electrostatic potential fit, local reference axis systems, and conformational dependence. *J. Comput. Chem.* **2012**, *33*, 1673–1688.
- (16) Bereau, T.; Kramer, C.; Meuwly, M. Leveraging Symmetries of Static Atomic Multipole Electrostatics in Molecular Dynamics Simulations. *J. Chem. Theory Comput.* **2013**, *9*, 5450–5459.
- (17) Kramer, C.; Bereau, T.; Spinn, A.; Liedl, K. R.; Gedeck, P.; Meuwly, M. Deriving Static Atomic Multipoles from the Electrostatic Potential. 2013.
- (18) Devereux, M.; Raghunathan, S.; Fedorov, D. G.; Meuwly, M. A Novel, Computationally Efficient Multipolar Model Employing Distributed Charges for Molecular Dynamics Simulations. *J. Chem. Theory Comput.* **2014**, *10*, 4229–4241.
- (19) Unke, O. T.; Devereux, M.; Meuwly, M. Minimal distributed charges: Multipolar quality at the cost of point charge electrostatics. *J. Chem. Phys.* **2017**, *147*, 161712.
- (20) Vanommeslaeghe, K.; MacKerell, A. D., Jr. CHARMM additive and polarizable force fields for biophysics and computer-aided drug design. *Biochimica et Biophysica Acta - General Subjects* **2015**, *1850*, 861–871.
- (21) Nutt, D.; Meuwly, M. Theoretical investigation of infrared spectra and pocket dynamics of photodissociated carbonmonoxy Myoglobin. *Biophys. J.* **2003**, *85*, 3612–3623.
- (22) Ren, P.; Ponder, J. Polarizable atomic multipole water model for molecular mechanics simulation. *J. Phys. Chem. B* **2003**, *107*, 5933–5947.

- (23) Wang, L.-P.; Head-Gordon, T.; Ponder, J. W.; Ren, P.; Chodera, J. D.; Eastman, P. K.; Martinez, T. J.; Pande, V. S. Systematic Improvement of a Classical Molecular Model of Water. *J. Phys. Chem. B* **2013**, *117*, 9956–9972.
- (24) Stone, A. J. Distributed multipole analysis: Stability for large basis sets. *J. Chem. Theory Comput.* **2005**, *1*, 1128–1132.
- (25) Kramer, C.; Gedeck, P.; Meuwly, M. Atomic Multipoles: Electrostatic Potential Fit, Local Reference Axis Systems and Conformational Dependence. *J. Comput. Chem.* **2012**, *33*, 1673–1688.
- (26) Bereau, T.; Kramer, C.; Meuwly, M. Leveraging Symmetries of Static Atomic Multipole Electrostatics in Molecular Dynamics Simulations. *J. Chem. Theory Comput.* **2013**, *9*, 5450–5459.
- (27) Troester, P.; Lorenzen, K.; Schwoerer, M.; Tavan, P. Polarizable Water Models from Mixed Computational and Empirical Optimization. *J. Phys. Chem. B* **2013**, *117*, 9486–9500.
- (28) Bertie, J.; Lan, Z. Infrared intensities of liquids .20. The intensity of the OH stretching band of liquid water revisited, and the best current values of the optical constants of H₂O(1) at 25 degrees C between 15,000 and 1 cm⁻¹. *Appl. Spectr.* **1996**, *50*, 1047–1057.
- (29) Sidler, D.; Meuwly, M.; Hamm, P. An efficient water force field calibrated against intermolecular THz and Raman spectra. *J. Chem. Phys.* **2018**, *148*, 244504.
- (30) Kumar, R.; Skinner, J. L. Water simulation model with explicit three-molecule interactions. *J. Phys. Chem. B* **2008**, *112*, 8311–8318.
- (31) Huang, X.; Braams, B.; Bowman, J. Ab initio potential energy and dipole moment surfaces of (H₂O)₂. *J. Phys. Chem. A* **2006**, *110*, 445–451.

- (32) Naserifar, S.; Goddard, W. A., III The quantum mechanics-based polarizable force field for water simulations. *J. Chem. Phys.* **2018**, *149*, 174502.
- (33) Babin, V.; Leforestier, C.; Paesani, F. Development of a “First Principles” Water Potential with Flexible Monomers: Dimer Potential Energy Surface, VRT Spectrum, and Second Virial Coefficient. *J. Chem. Theory Comput.* **2013**, *9*, 5395–5403.
- (34) Rein, R. On physical properties and interactions of polyatomic molecules with application to molecular recognition in biology. *Adv. Quantum Chem.* **1973**, *7*, 335–397.
- (35) Maroulis, G. Electric polarizability and hyperpolarizability of carbon monoxide. *J. Phys. Chem.* **1996**, *100*, 13466–13473.
- (36) Roco, J. M. M.; Calvo Hernandez, A.; Velasco, S. Far-Infrared Permanent and Induced Dipole Absorption of Diatomic Molecules in Rare-Gas Fluids. I. Spectral Theory. *J. Chem. Phys.* **1995**, *103*, 9161–9174.
- (37) Roco, J. M. M.; Medina, A.; Calvo Hernandez, A.; Velasco, S. Far-Infrared Permanent and Induced Dipole Absorption of Diatomic Molecules in Rare-gas Fluids. II. Application to the COAr System. *J. Chem. Phys.* **1995**, *103*, 9175–9186.
- (38) Straub, J. E.; Karplus, M. Molecular dynamics study of the photodissociation of carbon monoxide from myoglobin - Ligand dynamics in the 1st 10 ps. *Chem. Phys.* **1991**, *158*, 221–248.
- (39) Nutt, D.; Meuwly, M. CO migration in native and mutant Myoglobin: Atomistic simulations for the understanding of protein function. *Proc. Natl. Acad. Sci. USA* **2004**, *101*, 5998–6002.
- (40) Plattner, N.; Meuwly, M. The Role of Higher CO-Multipole Moments in Understanding the Dynamics of Photodissociated Carbonmonoxide in Myoglobin. *Biophys. J.* **2008**, *94*, 2505–2515.

- (41) Clark, T.; Hennemann, M.; Murray, J.; Politzer, P. Halogen bonding: the σ -hole. *J. Mol. Model.* **2007**, *13*, 291–296.
- (42) Murray, J.; Lane, P.; Politzer, P. Expansion of the σ -hole concept. *J. Mol. Model.* **2009**, *15*, 723–729.
- (43) Politzer, P.; Murray, J. S.; Clark, T. Halogen bonding: an electrostatically-driven highly directional noncovalent interaction. *Phys. Chem. Chem. Phys.* **2010**, *12*, 7748–7757.
- (44) Jackson, J. D. *Classical Electrodynamics*; John Wiley & Sons: New York, 1998.
- (45) Penney, W. The electronic structure of some polyenes and aromatic molecules. III. Bonds of fractional order by the pair method. *Proc. R. Soc. Lon. Ser. A - Math. Phys. Sci.* **1937**, *158*, 0306–0324.
- (46) Pauling, L. Atomic radii and interatomic distances in metals. *J. Am. Chem. Soc.* **1947**, *69*, 542–553.
- (47) Johnston, H. S.; Parr, C. Activation Energies from Bond energies. I. Hydrogen Transfer Reactions. *J. Am. Chem. Soc.* **1963**, *85*, 2544–2551.
- (48) van Duin, A. C. T.; Dasgupta, S.; Lorant, F.; Goddard III, W. A. ReaxFF: A Reactive Force field for hydrocarbons. *J. Phys. Chem. A* **2001**, *105*, 9396–9409.
- (49) Chenoweth, K.; van Duin, A. C. T.; Goddard, W. A., III ReaxFF reactive force field for molecular dynamics simulations of hydrocarbon oxidation. *J. Phys. Chem. A* **2008**, *112*, 1040–1053.
- (50) Senftle, T. P.; Hong, S.; Islam, M. M.; Kylasa, S. B.; Zheng, Y.; Shin, Y. K.; Junkermeier, C.; Engel-Herbert, R.; Janik, M. J.; Aktulga, H. M.; Verstraelen, T.; Grama, A.; van Duin, A. C. T. The ReaxFF reactive force-field: development, applications and future directions. *NPJ Comp. Mater.* **2016**, *2*, UNSP 15011.

- (51) Warshel, A.; Weiss, R. M. An empirical valence bond approach for comparing reactions in solutions and in enzymes. *J. Am. Chem. Soc.* **1980**, *102*, 6218–6226.
- (52) Glowacki, D. R.; Orr-Ewing, A. J.; Harvey, J. N. Non-equilibrium reaction and relaxation dynamics in a strongly interacting explicit solvent: $F + CD_3CN$ treated with a parallel multi-state EVB model. *J. Chem. Phys.* **2015**, *143*, 044120.
- (53) Valero, R.; Song, L.; Gao, J.; Truhlar, D. G. Perspective on Diabatic Models of chemical reactivity as illustrated by the gas-phase S_N2 reaction of acetat ion with 1,2-Dichloroethane. *J. Chem. Theory Comput.* **2009**, *5*, 1–22.
- (54) Valero, R.; Song, L.; Gao, J.; Truhlar, D. G. Erratum: Perspective on Diabatic Models of chemical reactivity as illustrated by the gas-phase S_N2 reaction of acetat ion with 1,2-Dichloroethane. *J. Chem. Theory Comput.* **2009**, *5*, 2191–2191.
- (55) Kamerlin, S. C. L.; Cao, J.; Rosta, E.; Warshel, A. On Unjustifiably misrepresenting the EVB approach while simultaneously adopting it. *J. Phys. Chem. B* **2009**, *113*, 10905–10915.
- (56) Hong, G.; Rosta, E.; Warshel, A. Using the constrained DFT approach in generating diabatic surfaces and off diagonal empirical valence bond terms for modeling reactions in condensed phases. *J. Phys. Chem. B* **2006**, *110*, 19570–19574.
- (57) Warshel, A. Dynamics of enzymatic reactions. *Proc. Natl. Acad. Sci. USA* **1984**, *81*, 444–448.
- (58) Strajbl, M.; Hong, G.; Warshel, A. Ab initio QM/MM simulation with proper sampling: "First principle" calculations of the free energy of the autodissociation of water in aqueous solution. *J. Phys. Chem. B* **2002**, *106*, 13333–13343.
- (59) Greaves, S. J.; Rose, R. A.; Oliver, T. A. A.; Glowacki, D. R.; Ashfold, M. N. R.; Harvey, J. N.; Clark, I. P.; Greetham, G. M.; Parker, A. W.; Towrie, M.; Orr-Ewing, A. J.

- Vibrationally Quantum-State-Specific Reaction Dynamics of H Atom Abstraction by CN Radical in Solution. *Science* **2011**, *331*, 1423–1426.
- (60) Glowacki, D. R.; Rose, R. A.; Greaves, S. J.; Orr-Ewing, A. J.; Harvey, J. N. Ultrafast energy flow in the wake of solution-phase bimolecular reactions. *Nat. Chem.* **2011**, *3*, 850–855.
- (61) Glowacki, D. R.; Rodgers, W. J.; Shannon, R.; Robertson, S. H.; Harvey, J. N. Reaction and relaxation at surface hotspots: using molecular dynamics and the energy-grained master equation to describe diamond etching. *Proc. R. Soc. Lon. Ser. A - Math. Phys. Sci.* **2017**, *375*, 20160206.
- (62) Chang, Y.-T.; Miller, W. H. An empirical valence bond model for constructing global potential energy surfaces for chemical reactions of polyatomic molecular systems. *J. Phys. Chem.* **1990**, *94*, 5884–5888.
- (63) Schmitt, U.; Voth, G. Multistate empirical valence bond model for proton transport in water. *J. Phys. Chem. B* **1998**, *102*, 5547–5551.
- (64) Schlegel, H. B.; Sonnenberg, J. L. Empirical valence-bond models for reactive potential energy surfaces using distributed Gaussians. *J. Chem. Theory Comput.* **2006**, *2*, 905–911.
- (65) Petrich, J. W.; Lambry, J. C.; Kuczera, K.; Karplus, M.; Poyart, C.; Martin, J. L. Ligand binding and protein relaxation in heme proteins: a room temperature analysis of nitric oxide geminate recombination. *Biochemistry* **1991**, *30*, 3975–3987.
- (66) Kruglik, S. G.; Yoo, B.-K.; Franzen, S.; Vos, M. H.; Martin, J.-L.; Negrerie, M. Picosecond primary structural transition of the heme is retarded after nitric oxide binding to heme proteins. *Proc. Natl. Acad. Sci. USA* **2010**, *107*, 13678–13683.

- (67) Kim, J.; Park, J.; Lee, T.; Lim, M. Dynamics of Geminate Rebinding of NO with Cytochrome c in Aqueous Solution Using Femtosecond Vibrational Spectroscopy. *J. Phys. Chem. B* **2012**, *116*, 13663–13671.
- (68) Yoo, B.-K.; Kruglik, S. G.; Lamarre, I.; Martin, J.-L.; Negrerie, M. Absorption Band III Kinetics Probe the Picosecond Heme Iron Motion Triggered by Nitric Oxide Binding to Hemoglobin and Myoglobin. *J. Phys. Chem. B* **2012**, *116*, 4106–4114.
- (69) Vaida, V.; Kjaergaard, H. G.; Hintze, P. E.; Donaldson, D. J. Photolysis of sulfuric acid vapor by visible solar radiation. *Science* **2003**, *299*, 1566 – 1568.
- (70) Crowther, A. C.; Carrier, S. L.; Preston, T. J.; Crim, F. F. Time-Resolved Studies of the Reactions of CN Radical Complexes with Alkanes, Alcohols, and Chloroalkanes. *J. Phys. Chem. A* **2009**, *113*, 3758–3764.
- (71) Hundt, P. M.; Jiang, B.; van Reijzen, M. E.; Guo, H.; Beck, R. D. Vibrationally Promoted Dissociation of Water on Ni(111). *Science* **2014**, *344*, 504–507.
- (72) Nutt, D. R.; Meuwly, M. Studying reactive processes with classical dynamics: Rebinding dynamics in MbNO. *Biophys. J.* **2006**, *90*, 1191–1201.
- (73) Danielsson, J.; Meuwly, M. Atomistic Simulation of Adiabatic Reactive Processes Based on Multi-State Potential Energy Surfaces. *J. Chem. Theory Comput.* **2008**, *4*, 1083.
- (74) Yosa Reyes, J.; Meuwly, M. Vibrationally Induced Dissociation of Sulfuric Acid (H₂SO₄). *J. Phys. Chem. A* **2011**, *115*, 14350–14360.
- (75) Nagy, T.; Yosa Reyes, J.; Meuwly, M. Multisurface Adiabatic Reactive Molecular Dynamics. *J. Chem. Theory Comput.* **2014**, *10*, 1366–1375.
- (76) Schmid, M. H.; Das, A. K.; Landis, C. R.; Meuwly, M. Multi-State VALBOND for

- Atomistic Simulations of Hypervalent Molecules, Metal Complexes, and Reactions. *J. Chem. Theory Comput.* **2018**, *14*, 3565–3578.
- (77) Landis, C. R.; Cleveland, T.; Firman, T. K. Valence Bond Concepts Applied to the Molecular Mechanics Description of Molecular Shapes. 3. Applications to Transition Metal Alkyls and Hydrides. *J. Am. Chem. Soc.* **1998**, *120*, 2641–2649.
- (78) Firman, T. K.; Landis, C. R. Valence bond concepts applied to the molecular mechanics description of molecular shapes. 4. Transition metals with pi-bonds. *J. Am. Chem. Soc.* **2001**, *123*, 11728–11742.
- (79) Tubert-Brohman, I.; Schmid, M.; Meuwly, M. A molecular mechanics force field for octahedral organometallic compounds with inclusion of the trans influence. *J. Chem. Theory Comput.* **2009**, *5*, 530.
- (80) Lammers, S.; Lutz, S.; Meuwly, M. Reactive force fields for proton transfer dynamics. *J. Comput. Chem.* **2008**, *29*, 1048–1063.
- (81) Mackeprang, K.; Xu, Z.-H.; Maroun, Z.; Meuwly, M.; Kjaergaard, H. G. Spectroscopy and dynamics of double proton transfer in formic acid dimer. *Phys. Chem. Chem. Phys.* **2016**, *18*, 24654–24662.
- (82) Xu, Z.-H.; Meuwly, M. Vibrational Spectroscopy and Proton Transfer Dynamics in Protonated Oxalate. *J. Phys. Chem. A* **2017**, *121*, 5389–5398.
- (83) Karandashev, K.; Xu, Z.-H.; Meuwly, M.; Vanicek, J.; Richardson, J. O. Kinetic isotope effects and how to describe them. *Struct. Dyn.* **2017**, *4*, 061501.
- (84) Xu, Z.-H.; Meuwly, M. Multistate Reactive Molecular Dynamics Simulations of Proton Diffusion in Water Clusters and in the Bulk. *J. Phys. Chem. B* **2019**, *123*, 9846–9861.
- (85) Hamm, P.; Lim, M.; DeGrado, W.; Hochstrasser, R. The two-dimensional IR nonlinear

- spectroscopy of a cyclic penta-peptide in relation to its three-dimensional structure. *Proc. Natl. Acad. Sci. USA* **1999**, *96*, 2036–2041.
- (86) Suydam, I. T.; Snow, C. D.; Pande, V. S.; Boxer, S. G. Electric fields at the active site of an enzyme: Direct comparison of experiment with theory. *Science* **2006**, *313*, 200–204.
- (87) Mondal, P.; Meuwly, M. Vibrational Stark spectroscopy for assessing ligand-binding strengths in a protein. *Phys. Chem. Chem. Phys.* **2017**, *19*, 16131–16143.
- (88) Lim, M.; Jackson, T. A.; Anfinrud, P. A. Mid-infrared vibrational spectrum of CO after photodissociation from heme: evidence of a docking site in the heme pocket of hemoglobin and myoglobin. *J. Chem. Phys.* **1995**, *102*, 4355.
- (89) Park, E. S.; Andrews, S. S.; Hu, R. B.; Boxer, S. G. Vibrational Stark Spectroscopy in Proteins: A Probe and Calibration for Electrostatic Fields. *J. Phys. Chem. B* **1999**, *103*, 9813–9817.
- (90) Ma, J.; Huo, S.; Straub, J. Molecular Dynamics Simulation Study of the B-States of Solvated Carbon Monoxymyoglobin. *J. Am. Chem. Soc.* **1997**, *119*, 2541–2551.
- (91) Meller, J.; Elber, R. Computer simulations of carbon monoxide photodissociation in myoglobin: Structural interpretation of the B states. *Biophys. J.* **1998**, *74*, 789–802.
- (92) Anselmi, M.; Aschi, M.; Di Nola, A.; Amadei, A. Theoretical Characterization of Carbon Monoxide Vibrational Spectrum in Sperm Whale Myoglobin Distal Pocket. *Biophys. J.* **2007**, *92*, 3442–3447.
- (93) Nienhaus, K.; Olson, J.; Franzen, S.; Nienhaus, G. The origin of stark splitting in the initial photoproduct state of MbCO. *J. Am. Chem. Soc.* **2005**, *127*, 40–41.
- (94) Meuwly, M. On the influence of the local environment on the CO stretching frequencies

- in native myoglobin: Assignment of the B-States in MbCO. *ChemPhysChem* **2006**, *7*, 2061–2063.
- (95) Wang, Y.; Huang, X.; Shepler, B. C.; Braams, B. J.; Bowman, J. M. Flexible, ab initio potential, and dipole moment surfaces for water. I. Tests and applications for clusters up to the 22-mer. *J. Chem. Phys.* **2011**, *134*, 094509.
- (96) Medders, G. R.; Babin, V.; Paesani, F. Development of a “First-Principles” Water Potential with Flexible Monomers. III. Liquid Phase Properties. *J. Chem. Theory Comput.* **2014**, *10*, 2906–2910.
- (97) Medders, G. R.; Paesani, F. Infrared and Raman Spectroscopy of Liquid Water through “First-Principles” Many-Body Molecular Dynamics. *J. Chem. Theory Comput.* **2015**, *11*, 1145–1154.
- (98) Braams, B. J.; Bowman, J. M. Permutationally invariant potential energy surfaces in high dimensionality. *Intern. Rev. Phys. Chem.* **2009**, *28*, 577–606.
- (99) Liu, H.; Wang, Y.; Bowman, J. M. Quantum calculations of the IR spectrum of liquid water using ab initio and model potential and dipole moment surfaces and comparison with experiment. *J. Chem. Phys.* **2015**, *142*, 194502.
- (100) Cazade, P.-A.; Bereau, T.; Meuwly, M. Computational Two-Dimensional Infrared Spectroscopy without Maps: N-Methylacetamide in Water. *J. Phys. Chem. B* **2014**, *118*, 8135–8147.
- (101) Cazade, P.-A.; Tran, H.; Bereau, T.; Das, A. K.; Klaesi, F.; Hamm, P.; Meuwly, M. Solvation of fluoro-acetonitrile in water by 2D-IR spectroscopy: A combined experimental-computational study. *J. Chem. Phys.* **2015**, *142*, 212415.
- (102) Lee, M. W.; Carr, J. K.; Goellner, M.; Hamm, P.; Meuwly, M. 2D IR spectra of cyanide

- in water investigated by molecular dynamics simulations. *J. Chem. Phys.* **2013**, *139*, 054506.
- (103) Desmond, J.; Koner, D.; Meuwly, M. Probing the Differential Dynamics of the Monomeric and Dimeric Insulin from Amide-I IR Spectroscopy. *J. Phys. Chem. B* **2019**, *123*, 6588–6598.
- (104) Salehi, S. M.; Koner, D.; Meuwly, M. Vibrational Spectroscopy of N_3^- in the Gas and Condensed Phase. *J. Phys. Chem. B* **2019**, *123*, 3282–3290.
- (105) Bernstein, F.; Koetzle, T.; Williams, G. J.; Jr., E. F. M.; Brice, M.; Rodgers, J.; Kennard, O.; Shimanouchi, T.; Tasumi, M. The protein data bank: A computer-based archival file for macromolecular structures. *J. Mol. Biol.* **1977**, *112*, 535–542.
- (106) Berman, H. M. et al. The protein data bank. *Biological Crystallography* **2002**, *58*, 899–907.
- (107) Baker, E. N.; Blundell, T. L.; Cutfield, J. F.; Dodson, E. J.; Dodson, G. G.; Hodgkin, D. M. C.; Hubbard, R. E.; Isaacs, N. W.; Reynolds, C. D.; Sakabe, K.; Sakabe, N.; Vijayan, N. M. The structure of 2Zn pig insulin crystals at 1.5 Å resolution. *Philos. Trans. R. Soc. London, Ser. B* **1988**, *319*, 369–456.
- (108) Jorgensen, W. L.; Chandrasekhar, J.; Madura, J. D.; Impey, R. W.; Klein, M. L. Comparison of Simple Potential Functions for Simulating Liquid Water. *J. Chem. Phys.* **1983**, *79*, 926–935.
- (109) Brooks, B. R. et al. CHARMM: The Biomolecular Simulation Program. *J. Comput. Chem.* **2009**, *30*, 1545–1614.
- (110) Klauda, J. B.; Venable, R. M.; Freites, J. A.; OConnor, J. W.; Tobias, D. J.; Mondragon-Ramirez, C.; Vorobyov, I.; MacKerell, A. D.; Pastor, R. W. Update of

- the CHARMM All-Atom Additive Force Field for Lipids: Validation on Six Lipid Types. *J. Phys. Chem. B* **2010**, *114*, 7830–7843.
- (111) Swope, W. C.; Andersen, H. C.; Berens, P. H.; Wilson, K. R. A Computer Simulation Method for the Calculation of Equilibrium Constants for the Formation of Physical Clusters of Molecules: Application to Small Water Clusters. *J. Chem. Phys.* **1982**, *76*, 637–649.
- (112) Nosé, S. A Unified Formulation of the Constant Temperature Molecular-Dynamics Methods. *J. Chem. Phys.* **1984**, *81*, 511–519.
- (113) Hoover, W. G. Canonical Dynamics: Equilibrium Phase-Space Distributions. *Phys. Rev. A* **1985**, *31*, 1695–1697.
- (114) Andersen, H. C. Molecular Dynamics Simulations at Constant Pressure and/or Temperature. *J. Chem. Phys.* **1980**, *72*, 2384–2393.
- (115) Nosé, S.; Klein, M. L. Constant Pressure Molecular Dynamics for Molecular Systems. *Mol. Phys.* **1983**, *50*, 1055–1076.
- (116) Hairer, E.; Lubich, C.; Wanner, G. Geometric Numerical Integration Illustrated by the Störmer/Verlet Method. *Acta Numerica* **2003**, *12*, 399–450.
- (117) Cazade, P.-A.; Hedin, F.; Xu, Z.-H.; Meuwly, M. Vibrational Relaxation and Energy Migration of N-Methylacetamide in Water: The Role of Nonbonded Interactions. *J. Phys. Chem. B* **2015**, *119*, 3112–3122.
- (118) Darden, T.; York, D.; Pedersen, L. Particle Mesh Ewald: An Nlog(N) Method for Ewald Sums in Large Systems. *J. Chem. Phys.* **1993**, *98*, 10089–10092.
- (119) Gunsteren, W. V.; Berendsen, H. Algorithms for Macromolecular Dynamics and Constraint Dynamics. *Mol. Phys.* **1997**, *34*, 1311–1327.

- (120) Ho, T.-S.; Rabitz, H. A General Method for Constructing Multidimensional Molecular Potential Energy Surfaces from Ab Initio Calculations. *J. Chem. Phys.* **1996**, *104*, 2584–2597.
- (121) Unke, O. T.; Meuwly, M. Toolkit for the Construction of Reproducing Kernel-Based Representations of Data: Application to Multidimensional Potential Energy Surfaces. *J. Chem. Inf. and Mod.* **2017**, *57*, 1923–1931.
- (122) Frisch, M. J. et al. Gaussian09 Revision D.01. Gaussian Inc. Wallingford CT 2009.
- (123) Colbert, D. T.; Miller, W. H. A Novel Discrete Variable Representation for Quantum Mechanical Reactive Scattering via the S-Matrix Kohn Method. *J. Chem. Phys.* **1992**, *96*, 1982–1991.
- (124) Woutersen, S.; Pfister, R.; Hamm, P.; Mu, Y.; Kosov, D. S.; Stock, G. Peptide Conformational Heterogeneity Revealed from Nonlinear Vibrational Spectroscopy and Molecular Dynamics Simulations. *J. Chem. Phys.* **2002**, *117*, 6833–6840.
- (125) Decamp, M. F.; Deflores, L.; Mccracken, J. M.; Tokmakoff, A.; Kwac, K.; Cho, M. Amide I Vibrational Dynamics of N-Methylacetamide in Polar Solvents : The Role of Electrostatic Interaction. *J. Phys. Chem. B* **2005**, *109*, 11016–11026.
- (126) Karplus, M.; Sharma, R. D.; Porter, R. N. Dynamics of Reactive Collisions - H + H₂ Exchange Reaction. *J. Chem. Phys.* **1964**, *40*, 2033–2034.
- (127) Schatz, G.; Kuppermann, A. Quantum-mechanical reactive scattering for 3-dimensional atom plus diatom systems .2. Accurate cross-sections for H+H₂. *J. Chem. Phys.* **1976**, *65*, 4668–4692.
- (128) London, F. Quantum mechanical interpretation of the process of activation. *Z. Elektrochem.* **1929**, *35*, 552–555.

- (129) Eyring, H.; Polanyi, M. Concerning simple gas reactions. *Z. Phys. Chem. Abt. B* **1931**, *12*, 279–311.
- (130) Sato, S. Potential energy surface of the system of three atoms. *J. Chem. Phys.* **1955**, *23*, 2465–2466.
- (131) Hutson, J. M. Intermolecular forces from the spectroscopy of Van der Waals molecules. *Ann. Rev. Phys. Chem.* **1990**, *41*, 123–154.
- (132) Hutson, J. M. An introduction to the dynamics of Van der Waals molecules. *Adv. Mol. Vibrat. Coll. Dyn.* **1991**, *1A*, 1–45.
- (133) Meuwly, M.; Hutson, J. The potential energy surface and near-dissociation states of He-H₂⁺. *J. Chem. Phys.* **1999**, *110*, 3418–3427.
- (134) Meuwly, M.; Hutson, J. M. Morphing ab initio potentials: a systematic study of Ne–HF. *J. Chem. Phys.* **1999**, *110*, 8338–8347.
- (135) Karman, T.; van der Avoird, A.; Groenenboom, G. C. Potential energy and dipole moment surfaces of the triplet states of the O₂ (*X*³Σ_g⁻) - O₂ (*X*³Σ_g⁻, *a*¹Δ_g, *b*¹Σ_g⁺) complex. *J. Chem. Phys.* **2017**, *147*, 084306.
- (136) Koner, D.; Veliz, J. C. S. V.; van der Avoird, A.; Meuwly, M. Near dissociation states for H₂⁺-He on MRCI and FCI potential energy surfaces. *Phys. Chem. Chem. Phys.* **2019**, *21*, 24976–24983.
- (137) Bender, J. D.; Doraiswamy, S.; Truhlar, D. G.; Candler, G. V. Potential energy surface fitting by a statistically localized, permutationally invariant, local interpolating moving least squares method for the many-body potential: Method and application to N-4. *J. Chem. Phys.* **2014**, *140*, 054302.

- (138) Tong, X.; Nagy, T.; Reyes, J. Y.; Germann, M.; Meuwly, M.; Willitsch, S. State-selected ion-molecule reactions with Coulomb-crystallized molecular ions in traps. *Chem. Phys. Lett.* **2012**, *547*, 1–8.
- (139) Hollebeek, T.; Ho, T.-S.; Rabitz, H. Constructing multidimensional molecular potential energy surfaces from ab initio data. *Annu. Rev. Phys. Chem.* **1999**, *50*, 537–570.
- (140) Koner, D.; Bemish, R. J.; Meuwly, M. The $\text{C}(^3\text{P}) + \text{NO}(\text{X}^2\Pi) \rightarrow \text{O}(^3\text{P}) + \text{CN}(\text{X}^2\Sigma^+)$, $\text{N}(^2\text{D})/\text{N}(^4\text{S}) + \text{CO}(\text{X}^1\Sigma^+)$ reaction: Rates, branching ratios, and final states from 15 K to 20000 K. *J. Chem. Phys.* **2018**, *149*, 094305.
- (141) Soloviov, M.; Meuwly, M. CO-dynamics in the active site of cytochrome c oxidase. *J. Chem. Phys.* **2014**, *140*, 145101.
- (142) Soloviov, M.; Das, A. K.; Meuwly, M. Structural Interpretation of Metastable States in Myoglobin-NO. *Angew. Chem. Int. Ed.* **2016**, *55*, 10126–10130.
- (143) Das, A. K.; Meuwly, M. Kinetic Analysis and Structural Interpretation of Competitive Ligand Binding for NO Dioxygenation in Truncated HemoglobinN. *Angew. Chem. Int. Ed.* **2018**, *57*, 3509–3513.
- (144) Sarma, G. Physico-chemical modelling in hypersonic flow simulation. *Progr. Aerospace Sci.* **2000**, *36*, 281–349.
- (145) Bertin, J.; Cummings, R. Fifty years of hypersonics: where we’ve been, where we’re going. *Prog. Aerospace Sci.* **2003**, *39*, 511–536.
- (146) Boyd, I. D.; Schwartzenuber, T. E. *Nonequilibrium Gas Dynamics and Molecular Simulation*; Cambridge University Press, New York, 2017.
- (147) San Vicente Veliz, J. C.; Koner, D.; Schwilk, M.; Bemish, R. J.; Meuwly, M. The $\text{N}(^4\text{S}) + \text{O}_2(\text{X}^3\Sigma) \leftrightarrow \text{O}(^3\text{P}) + \text{NO}(\text{X}^2\Pi)$ reaction: thermal and vibrational relaxation rates for the $^2\text{A}'$, $^4\text{A}'$ and $^2\text{A}''$ states. *Phys. Chem. Chem. Phys.* **2020**, *22*, 3927–3939.

- (148) Denis-Alpizar, O.; Bemish, R. J.; Meuwly, M. Reactive collisions for $\text{NO}(^2\Pi) + \text{N}(^4\text{S})$ at temperatures relevant to the hypersonic flight regime. *Phys. Chem. Chem. Phys.* **2017**, *19*, 2392.
- (149) Koner, D.; San Vicente Veliz, J. C.; ; Bemish, R. J.; Meuwly, M. Accurate Reproducing Kernel-Based Potential Energy Surfaces for the Triplet Ground States of N_2O and Dynamics for the $\text{N} + \text{NO} \leftrightarrow \text{O} + \text{N}_2$ Reaction. *arXiv preprint arXiv:2002.02310* **2020**,
- (150) Koner, D.; Bemish, R. J.; Meuwly, M. Dynamics on Multiple Potential Energy Surfaces: Quantitative Studies of Elementary Processes Relevant to Hypersonics. *arXiv preprint arXiv:2002.05087* **2020**,
- (151) Yosa Reyes, J.; Nagy, T.; Meuwly, M. Competitive reaction pathways in vibrationally induced photodissociation of H_2SO_4 . *Phys. Chem. Chem. Phys.* **2014**, *16*, 18533–18544.
- (152) Yosa Reyes, J.; Brickel, S.; Unke, O. T.; Meuwly, M. HSO_3Cl : a prototype molecule for studying OH-stretching overtone induced photodissociation. *Phys. Chem. Chem. Phys.* **2016**, *18*, 6780–6788.
- (153) Brickel, S.; Meuwly, M. OH-Stretching Overtone Induced Dynamics in HSO_3F from Reactive Molecular Dynamics Simulation. *J. Phys. Chem. A* **2017**, *121*, 5079–5087.
- (154) Brickel, S.; Meuwly, M. Molecular Determinants for Rate Acceleration in the Claisen Rearrangement Reaction. *J. Phys. Chem. B* **2019**, *123*, 448–456.
- (155) Rivero, U.; Unke, O. T.; Meuwly, M.; Willitsch, S. Reactive atomistic simulations of Diels-Alder reactions: The importance of molecular rotations. *J. Chem. Phys.* **2019**, *151*, 104301.
- (156) Nandi, A.; Qu, C.; Bowman, J. M. Full and fragmented permutationally invariant

- polynomial potential energy surfaces for trans and cis N-methyl acetamide and isomerization saddle points. *J. Chem. Phys.* **2019**, *151*, 084306.
- (157) Faber, F. A.; Christensen, A. S.; Huang, B.; von Lilienfeld, O. A. Alchemical and structural distribution based representation for universal quantum machine learning. *J. Chem. Phys.* **2018**, *148*, 241717.
- (158) Smith, J. S.; Isayev, O.; Roitberg, A. E. ANI-1: an extensible neural network potential with DFT accuracy at force field computational cost. *Chem. Sci.* **2017**, *8*, 3192–3203.
- (159) Schuett, K. T.; Sauceda, H. E.; Kindermans, P. J.; Tkatchenko, A.; Mueller, K. R. SchNet - A deep learning architecture for molecules and materials. *J. Chem. Phys.* **2018**, *148*, 241722.
- (160) Unke, O. T.; Meuwly, M. PhysNet: A Neural Network for Predicting Energies, Forces, Dipole Moments, and Partial Charges. *J. Chem. Theory Comput.* **2019**, *15*, 3678–3693.
- (161) Käser, S.; Unke, O. T.; Meuwly, M. Reactive Dynamics and Spectroscopy of Hydrogen Transfer from Neural Network-Based Reactive Potential Energy Surfaces. *New J. Phys.* **2020**, *in print*, in print.
- (162) Käser, S.; Unke, O. T.; Meuwly, M. Isomerization and Decomposition Reactions of Acetaldehyde Relevant to Atmospheric Processes from Dynamics Simulations on Neural Network-Based Potential Energy Surfaces. *arXiv preprint arXiv:2003:08171* **2020**,